How Fragile We Are: Influence of Stimulator of Interferon Genes (STING) Variants on Pathogen Recognition and Immune Response Efficiency

Jeremy Morere, Cécilia Hognon, Tom Miclot, Tao Jiang, Elise Dumont, Giampaolo Barone, Antonio Monari,* and Emmanuelle Bignon*

ACCESS | 📊 Metrics & More | 📖 Article Recommendations | 🆂🆈 Supporting Information

ABSTRACT: The stimulator of interferon genes (STING) protein is a cornerstone of the human immune response. Its activation by cGAMP in the presence of cytosolic DNA stimulates the production of type I interferons and inflammatory cytokines. In the human population, several STING variants exist and exhibit dramatic differences in their activity, impacting the efficiency of the host defense against infections. Understanding the molecular mechanisms of these variants opens perspectives for personalized medicine treatments against diseases such as viral infections, cancers, or autoinflammatory diseases. Through microsecond-scale molecular modeling simulations, contact analyses, and machine learning techniques, we reveal the dynamic behavior of four STING variants (wild type, G230A, R293Q, and G230A/R293Q) and rationalize the variability of efficiency observed experimentally. Our results show that the decrease in STING activity is linked to a stiffening of key structural elements of the binding cavity together with changes in the interaction patterns within the protein.

cGAS-STING Immune Pathway
STING Mutations -> Ligand accessibility
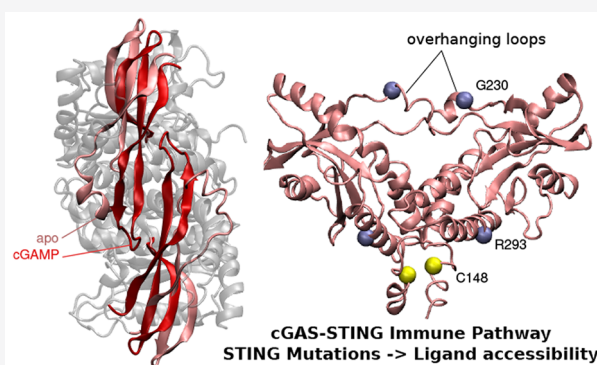
INTRODUCTION

The defenses of evolved organisms, including humans, against pathogenic infection rely on finely tuned biological machineries involving several cellular signaling mechanisms. The cyclic guanosine monophosphate—adenosine monophosphate synthase—stimulator of interferon genes (cGAS-STING) pathway is a key player that acts as a cytosolic DNA or RNA probe. After sensing the presence of genetic material, it triggers the immune response through the production of type I interferon and cytokines.[1,2] Indeed, the recognition of aberrant nucleic acid fragments in the cellular cytosol, such as those secreted by bacteria or resulting from viral infection, stimulates the cGAS enzyme, which produces cyclic guanosine adenosine monophosphate (cGAMP). Subsequently, cGAMP is sequestered by STING, inducing its activation and the final production of type I interferon and proinflammatory cytokines. These processes also cause the promotion of downstream inflammatory signaling for protection of uninfected cells and stimulation of the adaptive immune response.[3] As a consequence, STING is known to play a crucial and sometimes contrasting role in different biological responses, including antiviral defense,[3,4] mediation of tumor-suppressive and tumor-promoting mechanisms,[5−7] autophagy,[8,9] skin wound healing,[10] and the development of auto-inflammatory diseases.[11,12] Its delayed activation might also be involved in severe COVID-19 outcomes.[13,14]

In this context, it has also been underlined that over-stimulation of the cGAS-STING pathway leads to an inflammatory-like cytokine response, which is also strongly correlated with severe forms of the SARS-CoV-2 infection.[15] Hence, modulation of the cGAS-STING pathway and the related regulatory proteins provides suitable targets for the development of a wide variety of potential anticancer, antipathogen, and anti-inflammatory drugs.[16−19] Furthermore, modulation of the STING pathway could have an influence on the response to vaccines.

As a matter of fact, the structure of the human STING protein has been entirely resolved, and mechanistic hypotheses about its activation have been sketched so far.[20−22] STING is a transmembrane protein that is mainly localized in the endoplasmatic reticulum (ER) and is composed of two equivalent monomers. From a structural point of view, one can distinguish an N-terminal transmembrane domain having a high density of α-helices, a cytoplasm-exposed C-terminal
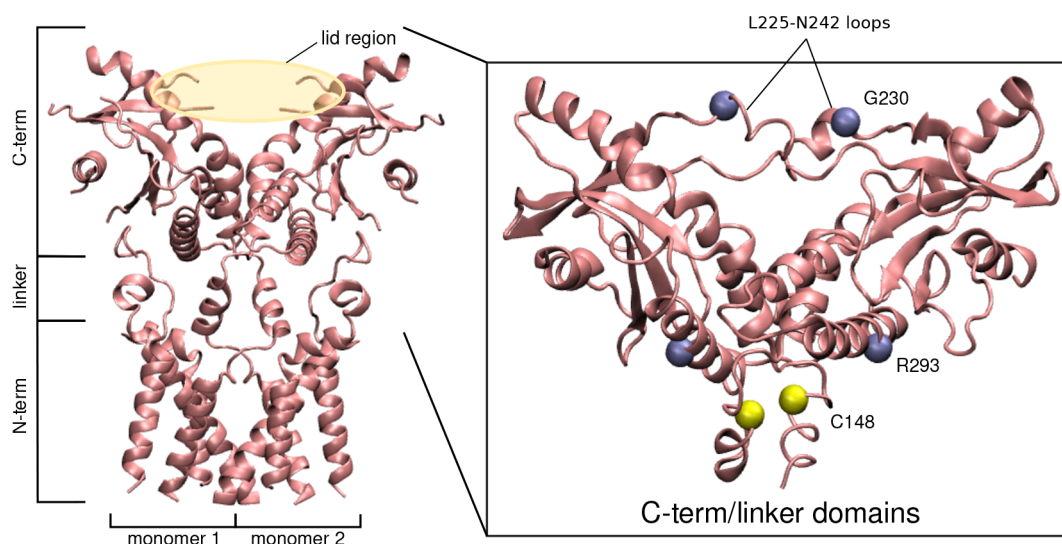
Figure 1. Cryo-EM structure of the full-length apo STING dimer (PDB ID 6NT5).[20] The magnified section shows the model used in our calculations, featuring the C-terminal and linker domains. The polymorphic sites and the cysteines involved in the tetramerization are depicted as violet and yellow beads, respectively.

domain containing the cGAMP binding site, and a short linker region connecting the two domains (Figure 1). Upon recognition and binding with cGAMP, the C-terminal domain undergoes an important structural reorganization that ultimately results in the tetramerization of two different STING dimers and hence in the activation of the immune response. The cGAMP binding site is constituted by a pocket in the C-terminal domain that is surrounded by overhanging tails (lid regions), forming flexible random coils in the apo form that stiffen into β-sheets in the presence of the ligand. Experimental and theoretical studies have stressed the importance of Arg232, Arg238, Tyr167, Ser241, Thr263, and Thr267 for stabilization of the ligand within the cavity.[21,23] From a biochemical point of view, STING polymerization, which is crucial for its full activation, takes place through the exposure of two cysteine residues (Cys148) in the linker domain, which leads to the formation of a disulfide bond bridging the two dimers.[21] The tetramerization efficiency strongly depends on the solvent accessibility of these residues, which are embedded in a rather flexible protein region that may nonetheless assume an α-helix arrangement. Their solvent exposure is also modulated by the shielding effects caused by the two disordered C-terminal tails, whose conformation can be strongly affected by the ligand-induced structural transition, further justifying the cGAMP-induced activation.

The STING-1 gene, also known as TMEM173, MPYS, MITA, ERIS, and NET23, codes for the STING protein and has a relatively high heterogeneity in the human population, which translates into the presence of several single-nucleotide polymorphisms involving the different domains of the protein. Although the R232 allele is the most common, it amounts to only ~60% of the general population, and many variants coexist: ~20% of the population harbor the triple-mutated R71H/G230A/R293Q (HAQ) variant, ~14% carry the R232H polymorphism, ~5% exhibit the G230A/R293Q (AQ) substitutions, and 2% have the R293Q substitution.[3,24] The activity of STING can differ from one variant to another, with possible loss of function associated with the HAQ and R232H variants and, contrarily, a gain of function with the N154S/V155M/V147L triple mutant, as found in patients suffering from vascular and pulmonary syndromes.[25] Indeed, these combined differ-

ences induce variability in exogenous DNA or RNA sensing and consequently in the response to pathogen infections. Notably, the HAQ and R232H genotypes are associated with poor outcomes in patients suffering from cervical cancer.[26] Individuals carrying the HAQ polymorphism are more likely to contract Legionnaires' disease,[27] probably more susceptible to infections, and less responsive to DNA vaccines.[28] Interestingly, the loss of function held by the HAQ variant might be mostly attributed to the R71H and R293Q substitutions, while the G230A polymorphism would help maintain a partial response to bacterial cyclic dinucleotides.[29] On the contrary, the R293Q substitution might provide enhanced protection against aging-associated diseases.[30] However, gain-of-function variants might also contribute to auto-inflammatory diseases development.

On the bases of all these considerations, we used state-of-the-art all-atom molecular dynamics (MD) simulations to unravel at an atomic resolution the effects of common mutations (G230A, R293Q and G230A/R293Q see Figure 1) on the structural transition induced on STING by cGAMP binding. The biophysical knowledge so obtained is related to the observed differences in STING activation and hence immune response efficiency. In particular we focus on the effects of the mutations on either the exposition of the dimerization site or the accessibility of the binding pocket. To this aim we resort to a truncated model of the protein involving only the cytoplasmatic C-terminal domain and the linker region. If this model, lacking the transmembrane domain, is not sufficient to fully describe the dimerization events, its reduced size allows a more extensive sampling of the rather complex interactions and long-range effects taking place upon cGAMP binding. Machine learning algorithms and contacts analysis were used to reveal both the key amino acids leading to the conformational transition and the allosteric consequences of the nucleotide mutations.

As a matter of fact, only a few theoretical studies dealing with MD simulations of mutated STING have been reported to date.[31−38] Notably, a study of the interaction of the agonist DMXAA on mouse STING and cyclic dinucleotide (CDN) screening studies are available in the literature.[31−37] Very recently, MD simulations were performed on a wild-type

STING model complexed with different CDNs, including cGAMP.[38] The binding was shown to induce conformational reorganization, as also suggested by dynamic network and cross-correlation analyses. The authors also suggested that while they could not directly relate their finding to the full activation mechanism, ligands favoring close and rigid conformations of STING should be beneficial for the activation. Our results for the first time provide a clear picture of the first steps of STING activation as well as its perturbation caused by common human variants such as the HAQ and AQ genotypes, which are associated with loss of function. More specifically, we pinpoint the role played by the global stiffening of the protein structure upon cGAMP recognition. Furthermore, we show how the combination of the different mutations involved in the HAQ variant leads to a drastic reorganization of the interaction network in the binding pocket that modulates the opening and closing of the protein, ultimately impacting cGAMP affinity and the immune response.

■ METHODS

System Setup. As mentioned in the Introduction, we chose a reduced model involving only the C-terminal domain of STING and the disordered linker region. Hence, we excluded from our model all of the N-terminal transmembrane domain. If this choice induces a drastic simplification of the model, it also allows us to employ a reduced-size system for which the statistical sampling will be deeper. In addition, it allows us to concentrate on the effects of cGAMP binding and mutations while neglecting the transmembrane effects. However, it is worth mentioning that although our model is suited to explore the stiffening of STING and the differential effects of the mutants, it lacks an important element, i.e., the N-terminal disordered tails that protrude outside the lipid membrane and are susceptible to interaction with the linker region, contributing to the modulation of the accessibility of the dimerization site. If we are aware of some of the biases induced by our choice, it is important to underline that the disordered chains could be included only in the presence of the full system, hence limiting the statistical sampling. Furthermore, capturing their disordered nature would be particularly challenging with a conventional force field, which could lead to nonphysical overstructuring of those domains. We should also stress once more that in this contribution we mainly want to understand the effects of the STING mutations on the binding capability and the linker domain structure.

For the apo systems, the starting structures were generated on the basis of the C-terminal and linker domains from the cryo-EM structure of full-length human STING (PDB ID 6NT5).[20] The missing loops were reconstructed using SwissModel.[39] The starting models for the systems with cGAMP were generated by combining the ligand binding domain of human cGAMP-bound STING (PDB ID 4KSY)[40] with the dimerization domain extracted from the structure of full chicken STING (PDB ID 6NT7).[20] From these starting structures, the variants were built by mutating residues 230 and/or 293 in silico. Force field parameters for the cGAMP ligand were generated using the antechamber module of AMBER18[41] for the derivation of RESP charges[42] and the attribution of GAFF parameters[43] (see the parameters in the Supporting Information). Standard STING residues were modeled using the Amber ff14SB force field.[44] The system was soaked in a cubic TIP3P water box with a 15 Å buffer, and potassium counterions were added to ensure a neutral total charge, resulting in systems of ~135 000 atoms.

The use of a minimal versus physiological salt concentration is clearly a debatable issue. However, in this case our choice is also justified by the fact that we are already using a truncated system missing the transmembrane domain and the lipid bilayer, a simplification that can be more important than the lack of physiological ionic strength.

Molecular Dynamics Simulations. MD simulations were carried out using NAMD3[45] for the dominant genotype of the human STING (wild type, WT) in its apo form and in the cGAMP-bound state. The hydrogen mass repartitioning (HMR) method was used to allow a 4 fs time step for the integration of the equations of motion. To prepare the system, 10 000 minimization steps were first performed with positional constraints imposed on the protein backbone. The minimization run was followed by 12 ns of equilibration at 300 K, during which the constraints were progressively released. The temperature was kept constant using the Langevin thermostat with a collision frequency of 1.0 ps^{-1}, and electrostatic interactions were treated using the particle mesh Ewald (PME) protocol.[46] After equilibration, the conformational ensemble was sampled along a 500 ns production run, and structures were dumped every 40 ps. The same protocol was used to sample three mutated states, involving the G230A (A-STING), R293Q (Q-STING), and G230A/R239Q (AQ-STING) mutations. The starting protein structures were built manually by performing the point mutations from the WT system. It should be noted that in the limit of our truncated system, AQ-STING can be considered as the highly spread and loss-of-function-inducing HAQ genotype.

Structural Analysis. The cpptraj module of AMBER18[41] was used to calculate distances, angles, and root-mean-square deviations (RMSD) and to perform the clustering analysis. The latter was carried out according to deviations of the protein backbone, and structures were clustered into five groups. The opening angle of the protein was computed as the angle involving the center of mass of the S162 residues lying at the bottom of the binding cavity and the residues forming the β-sheet of the upper lobe of each STING monomer (residues 197−204, 218−224, 242−261, and 308−314). The propensity of arginines to rotate into the cavity was computed with respect to their distance to the center of mass of the S162 residues. Contact-analysis changes upon mutations of STING were computed using the GetContacts software (https://getcontacts.github.io/). Frequencies of contacts were calculated for each pair of residues, and the most different patterns (75% threshold) identified among the STING variants were plotted as heat maps using the ggplot2 package of R.[47] Representations of the STING structure and projection of the contacts perturbation were rendered by VMD.[48]

Thermodynamic Integration. The perturbation of the free energy of binding upon mutation was assessed by thermodynamic integration (TI). The soft core potential method was used to progressively alchemically mutate G230 to A or R293 to Q. As the system is dimeric, each polymorphism implies two mutations in the system. To deal with this, we computed the ΔG for binding by computing the thermodynamic cycle for one mutation on the first monomer and then a second thermodynamic cycle adding the mutation on the second monomer. Free energy calculations on the AQ double mutant were carried out from the A system in two steps as well. Minimization for 10 000 steps, 60 ps of thermalization, and 1 ns production runs were performed with pmemd[41] along 11 windows with λ values
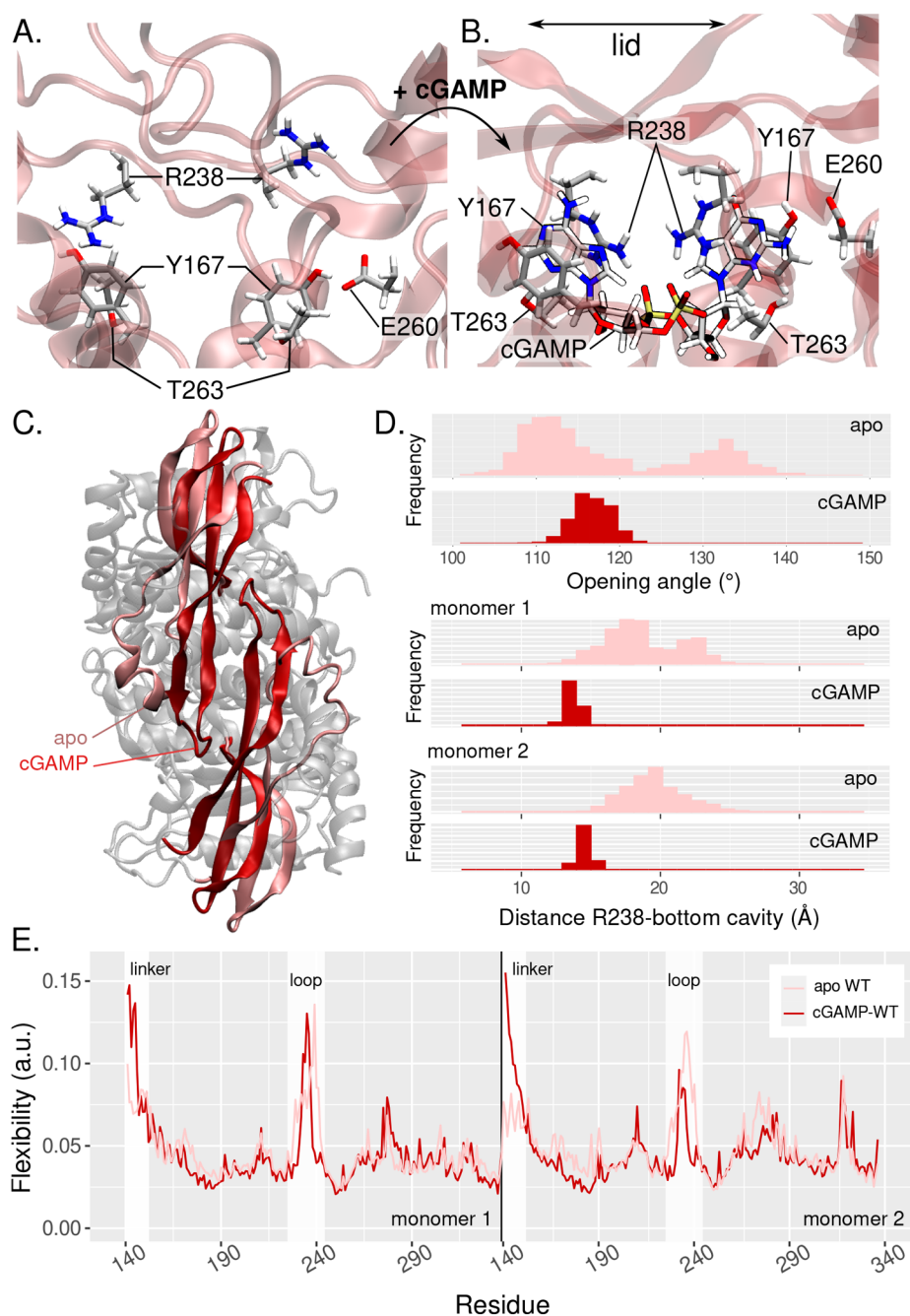
Figure 2. Perturbation of STING chemical and physical features upon cGAMP binding. Pink coloration corresponds to apo STING and dark-red coloration to STING bound to cGAMP. (A, B) Representative structures of the STING cavity (A) without and (B) with cGAMP. R238, Y167, T263, and E260 of each monomer form the first coordination sphere around the ligand. (C) Top view of the superimposed apo and complexed dimers. The lid region gets structured into β-sheets upon ligand binding. (D) Distributions of the opening angle and the distance between R238 and the bottom of the cavity. (E) Flexibility profiles of STING residues for the apo and complexed systems.

varying from 0.0 to 1.0, and the convergence was further checked.

Principal Component Analysis. Molecular dynamics simulation can provide important insights into the chemical and physical behaviors of proteins, but the large dimensionality of the data obtained sometimes makes it difficult to grasp the essence of the behavior of the model system. Principal component analysis (PCA) performs a linear mapping of the data to a lower-dimensional space by reconstructing a new configurational space that contains the most important degrees of freedom, providing a more intuitive way of understanding the

chemical processes involved. In practice, PCA creates a covariance matrix from the coordinates of the trajectory and then computes its eigenvectors and corresponding eigenvalues. These eigenvectors serve as basis vectors of a new configurational space, with each of them being a direction of motion. The first few eigenvectors with the highest eigenvalues are called principal components (PCs), and they often contribute to the vast majority of the system's behavior. In this paper, the sklearn library was used with a home-brew script to perform PCA. We used the internal coordinates (inverse distances between geometric centers of two residues) of the trajectories as the
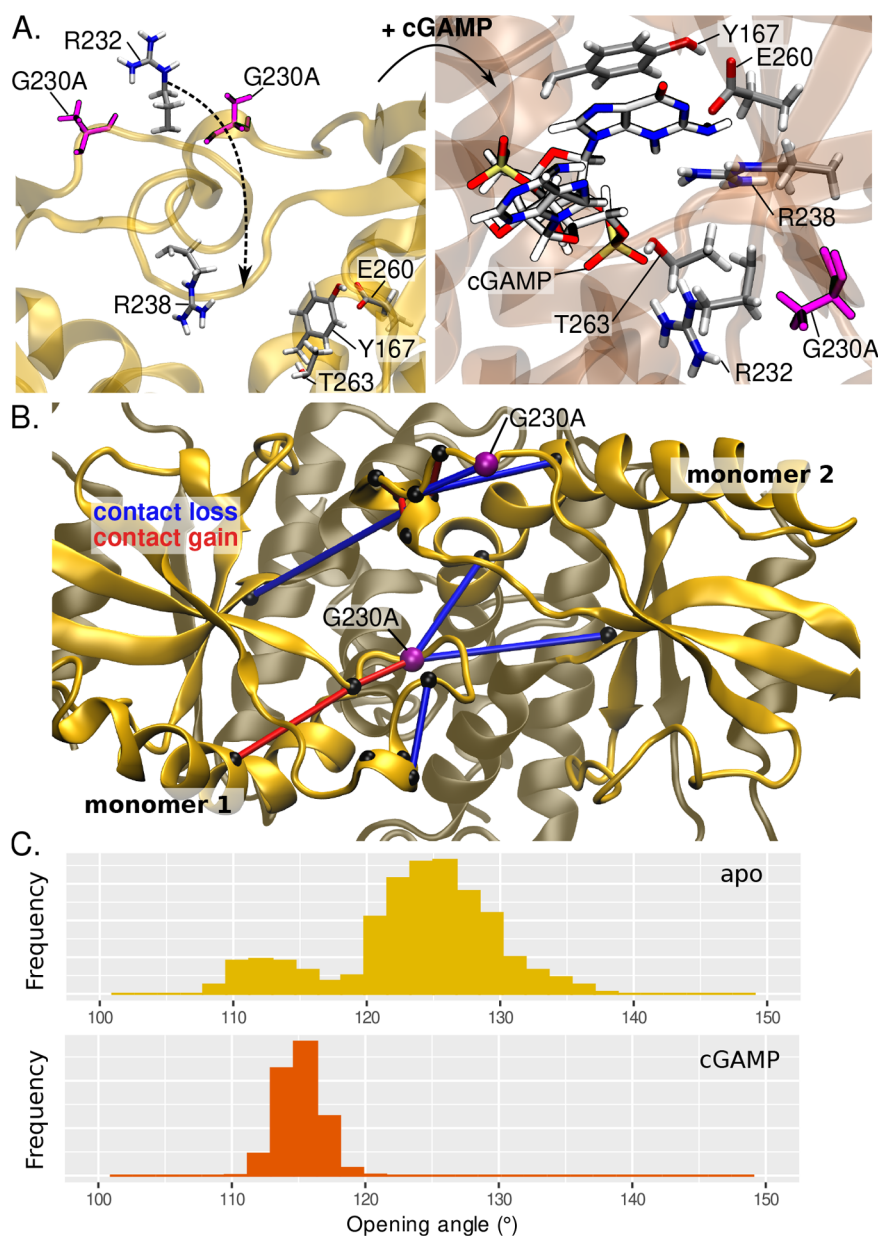
Figure 3. (A) (left) Structure of the A variant in the apo state. The mutated residues G230A of both monomers are depicted in purple licorice, and the residues interacting with the guanosine moiety of cGAMP upon binding are displayed in licorice. (right) Zoomed view of the interactions with the guanosine within the binding cavity of the cGAMP-bound structure. R232 rotates inward to interact with the phosphate. (B) Projection of the main changes of contacts in the lid region of apo STING upon G230A mutation (top view). Loss and gain of contacts are represented as blue and red tubes, respectively. The amino acids involved in the perturbed contacts are depicted as black beads and the G230A mutations as purple beads. (C) Opening angle distributions for the apo and cGAMP-bound states of A-STING.

input of PCA instead of the Cartesian coordinates to provide better performance.[49] The per-residue importance was calculated by taking the sum of the weights of the PCs up to 80%, where the weight is defined as the eigenvalue of the corresponding PC over the sum of all the eigenvalues.

Data and Software Availability. The supporting data described below are available online and can also be found in our GitHub repository: https://github.com/emmanuellebignon/STINGvariants-data. All of the software products used to perform this study are available online.

■ RESULTS AND DISCUSSION

Structural Features of STING upon Activation by cGAMP. *Organization of the Binding Cavity.* In the apo state, STING experiences structural fluctuations between the open and closed states, with the L225−N242 loops overhanging the binding cavity exhibiting high flexibility (Figures 1 and S1). Only D237 and R238 in the loops appear to be able to form stable interactions with K224, Y240, S241, N242, E260, or Y245 on the facing monomer. Nevertheless, the loops remain disordered along the trajectory. The overall structure fluctuates between two opening states in the apo form, as shown in Figure 2A and by the two-maximum distribution of the opening angle shown in Figure 2D (around either 110° or 135°). The angle is
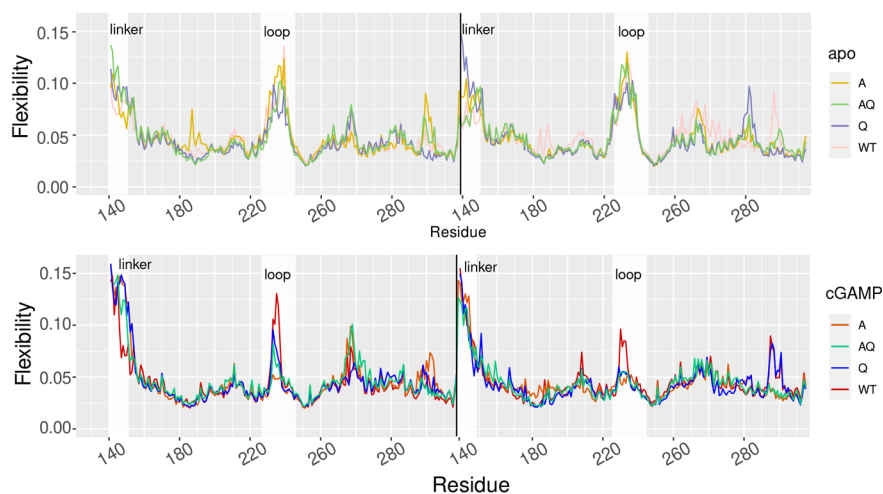
Figure 4. Flexibility profiles of the variants (WT, A, Q, AQ) in the (top) apo and (bottom) cGAMP-complexed states.

instead stabilized at $116.7 \pm 0.1°$ by cGAMP binding, leading to a stable closed conformation, as shown in Figure 2B. Upon binding of cGAMP, the two loops fold onto the ligand to structure into "lids" at the edges of the binding cavity, as observed in previous experimental and theoretical studies.[20,21,23,31] Two arginines belonging to the loops (R238 on each monomer) rotate toward cGAMP and get stabilized by strong cation−π interactions with the purine moieties of cGAMP; the distances between the purine nucleobase and the arginine side chains are 3.29 ± 0.25 and 5.01 ± 0.41 Å for the first and second monomers, respectively (Figures 2B and S2). The extremities of the loops forming the lid region get stabilized by interacting with the facing α-helix, which results in a very stable β-sheet conformation of the lid. At the extremity of both loops, D210 forms salt bridges with K236 (4.53 ± 1.80 Å between K236 NZ and D210 CG) and R232 (less persistent, 6.50 ± 3.00 Å between R232 CZ and D210 CG), and hydrophobic interactions involving L180, A243, I245, P199, and V198 are also observed along the trajectory.

Globally the binding of cGAMP induces a very stable interaction network in the binding pocket. The latter involves, in addition to the R238 cation−π interactions already described, π stacking of Y167 with the cGAMP purines. Furthermore, hydrogen bonds between R238 and the ligand's phosphates and between the nucleobases and E260 and T263 also emerge (Figure 2). These residues were previously proposed to take part in cGAMP recognition,[31] and we also retrieve the previously reported amino acids T267 in the second sphere of interaction together with Y163 and Y240 (Figure S3). The R232 residues invoked in the literature[23] are instead located on the external face of the lid and stay relatively far from cGAMP all along the trajectory in the WT. However, as will be discussed in the following, they play a more important role in the A and AQ variants. Interestingly, the S162 residue of both monomers, which lies at the bottom of the cavity and whose mutation to T or A destabilizes the cGAMP:STING complex,[31] is also involved in the second sphere of interaction in our simulations.

Flexibility Profile. In order to further probe the perturbation of the physical and structural properties resulting from the binding of cGAMP, we used a machine learning protocol based on principal component analysis to postprocess the MD trajectory and determine the flexibility profile of the protein. We have successfully used this methodology on other DNA and protein model systems.[50−52] The comparison of the WT STING flexibility profiles in the apo and cGAMP-bound states underlines the stiffening of the lid region (residues 225−240) coupled to its structuring into a stable β-sheet as a result of the arginines diving toward the ligand (Figure 2E). Interestingly, one can instead distinguish enhanced flexibility in the cytosol−transmembrane linker region opposite to the binding pocket, which harbors the cysteine residues that are involved in the disulfide bridge formation leading to the subsequent multimerization and STING activation. The assessment of the cysteine exposure to the solvent also shows an increase of the number of water molecules around these residues in the bound state, suggesting that the residues are more accessible and hence more prone to encounter the reactive partners (Figure S4). Nevertheless, as we used a truncated model in our simulations, this conclusion should be taken with some caution since we cannot fully conclude that the same behavior would happen in the full-length structure. However, the former stands as an interesting hypothesis concerning allosteric regulation of STING activation that deserves to be investigated in further studies.

Variant-Induced Changes in Chemical and Physical Properties. *G230A Variant.* Compared with the WT, the open conformation of the apo state is favored by this variant, as shown by the opening angle of $123.7 \pm 0.4°$. Indeed, in this case only a single maximum in the distribution of the opening angle is observed. This fact is mainly due to a loss of contacts between the lid region and the facing monomer (Figures 3A,C and S5).

Upon binding of cGAMP, the structure closes around the ligand, and the opening angle drops to $115.1 \pm 0.1°$, similar to what is observed for the WT (Figure 3B,C). The lid region becomes highly structured and exhibits the lowest flexibility of all the variants, with an enhanced and contrasted interaction network with respect to the WT (Figures 4 and S6). This observation is coherent with recent differential scanning fluorimetry (DST) results, which suggested that higher melting temperatures for the G230A cGAMP:STING complex might be related to structural stabilization of the lid region, as the ligand affinity of this variant is similar to that observed for the WT.[31] In line with these observations, the binding free energy change upon G230A mutation predicted by thermodynamic integration calculations is only 1.20 ± 0.25 kcal/mol (Table 1). Isothermal titration calorimetry (ITC) measurements also reported

negligible effect of the G230A mutation on cGAMP affinity for STING, which supports our results.[31]

Table 1. Relative Free Energies of Binding (ΔΔ*G*, in kcal/mol) upon Mutation of WT STING into the A, Q, and AQ Models as Computed by Thermodynamic Integration Calculations

variant	ΔΔ*G*	error
G230A	1.20	±0.25
R293Q	1.11	±0.65
G230A/R293Q	9.40	±0.68

On the contrary, the strongly enhanced structuration of the lid region upon cGAMP binding is well-evidenced by the flexibility profile (Figure 4). The stiffening of the lid impacts the organization of the binding site around cGAMP. On the guanosine side of the ligand, the G230A mutation hampers the interaction of R238 with cGAMP. R238 is pushed further from the purine than in the WT, yet it is proximal enough to interact with the phosphate by hydrogen bonds. Interestingly, the nucleobase position is mainly maintained by π stacking with Y167 and hydrogen bonding with E260. Contrary to the WT, R232 rotates toward the ligand to persistently interact with the phosphate group. T263 also interacts with the latter instead of the nucleobase as in the WT structure. On the adenosine side of cGAMP, one retrieves the π stacking of the nucleobase with Y167 and the hydrogen bond with T263 as well as the interaction between R238 and the phosphate, although R232 is again further from the nucleobase than what is found for the WT, preventing cation−π interactions (Figure 3). Altogether, the influence of the G230A mutation on STING function can be associated with the favoring of an open conformation in the apo state, which is ideal to ensure recognition and binding of cGAMP. Although the interaction network in the binding pocket is altered, the ligand is still stabilized, and the same increased flexibility and cysteine exposure in the linker region are observed (Figure S4). Hence, one can conclude that the presence of the G230A mutation should favor global STING activation.

R293Q Variant. In contrast to the previous case, the R239Q mutation is located further from the binding pocket. The Q-STING binding site harbors cGAMP in a similar fashion as the WT (Figure S7). Both R238 residues interact through cation−π interactions and hydrogen bonds with the nucleobases and the phosphates of cGAMP. E260, Y167, and T263 also participate in the interaction network within the cavity, and the R232 residues remain in the second sphere of interaction but point toward the bulk (Figure S3). Interestingly, in the apo state, both R238 residues form very stable hydrogen bonds with the E260 residues on the facing α-helices, which promotes a closed conformation characterized by an opening angle of $116.0 \pm 0.2°$ (Figure 5C). The more moderate opening of the binding pocket disfavors cGAMP access and hence its recognition (Figure 5A). Besides, for Q-STING the contact map underlines much more frequent interactions within the lid region itself and also with the surroundings spanning residues 225 to 240 in both monomers. Interestingly, these contacts are more pronounced than for the other variants and exhibit a contrasted pattern compared with WT-STING (Figure S5). Conversely, cGAMP binding still induces a considerable enhancement of the flexibility of the linker regions and hence a more solvent-exposed cysteine. As a consequence, and in particular because of the promotion of a
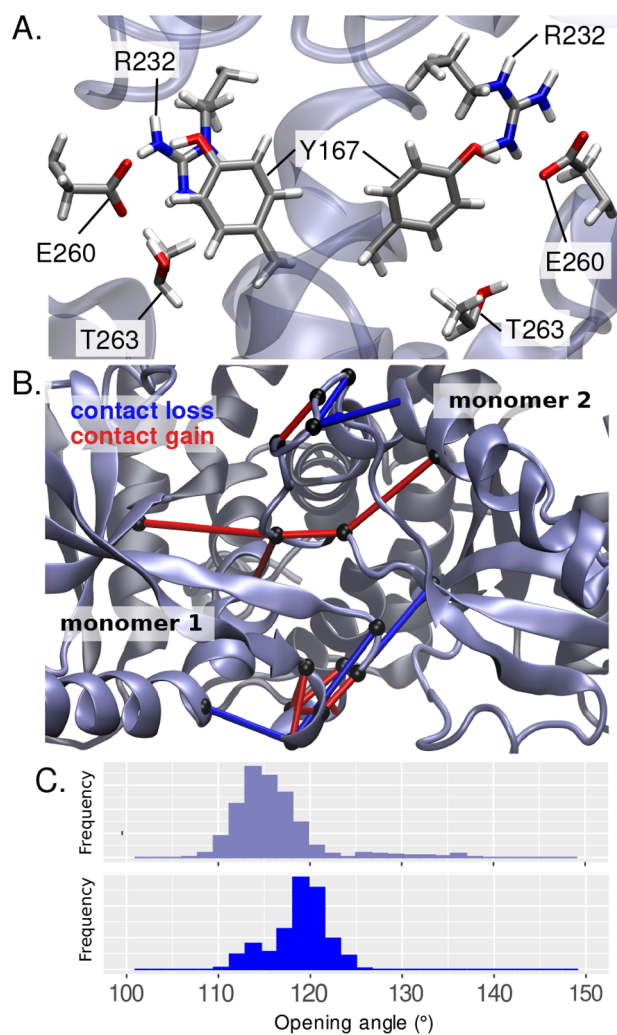

Figure 5. (A) Organization of the binding cavity in the apo R293Q variant. (B) Projection of the main changes of contacts in the lid region of apo STING upon R293Q mutation (top view). Loss and gain of contacts are represented as blue and red tubes, respectively. The amino acids involved in the contacts are depicted as black beads. (C) Opening angle distributions for the (top) apo and (bottom) cGAMP-bound states of Q-STING.

more closed conformation in the apo state that is susceptible to strongly perturb the recognition of cGAMP, this mutation should be correlated to a loss of activity of STING.

G230A/R293Q Variant. The AQ model, which may be directly related to the loss-of-function HAQ STING genotype, presents a binding site organization much like that of the A variant. In the apo form, Y167 is close to E260 and T263, while R238 remains in the cavity and R232 is in the bulk (Figure 6A).

Upon ligand binding, R232 rotates into the cavity and interacts with the phosphate group (Figure 6A). Contrary to the A variant, the π-stacking interaction with the guanosine is not disrupted, and R238 does not enter the cavity but rather interacts with the surface. We retrieve here the interactions between cGAMP and E260, Y167, and T263. Importantly, however, the opening angle distributions are centered around $122.4 \pm 0.1°$ and $113.9 \pm 0.1°$ in the apo and bound states, respectively (Figure 6C). Interestingly, the opening angle for the AQ variant lies in between those for the open and closed conformations observed in the other variants, and it exhibits the
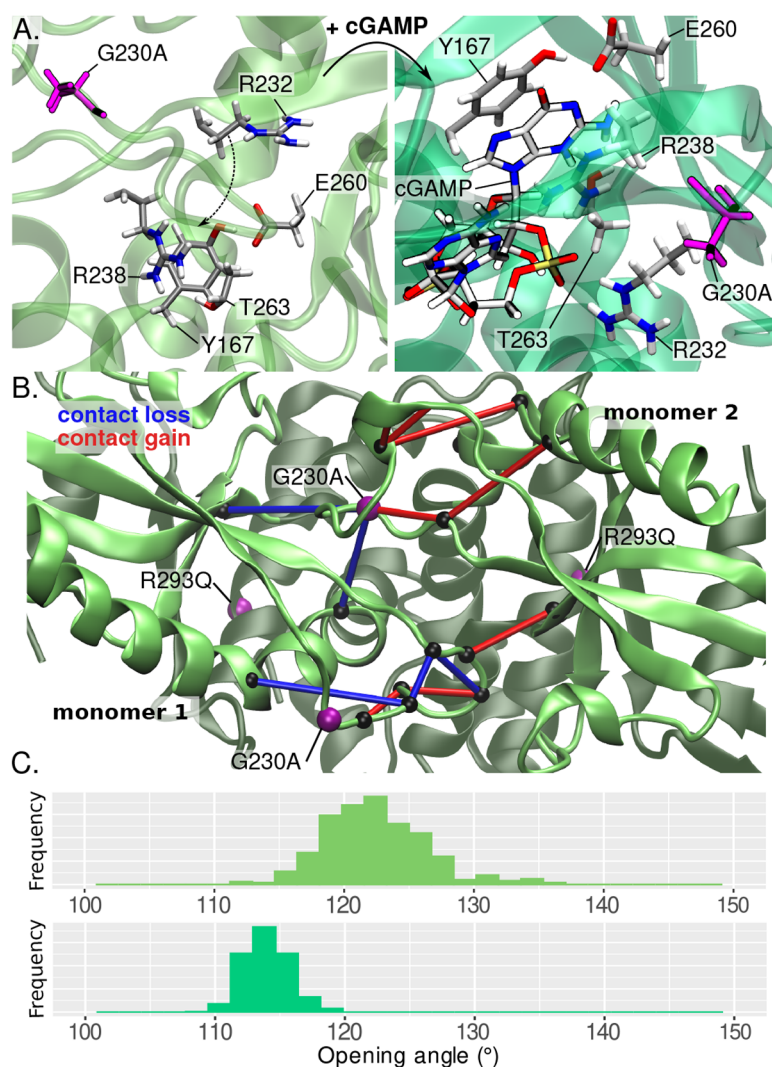
Figure 6. (A) (left) Organization of the binding cavity in the apo G230A/R293Q variant. The mutated G230A residue is depicted in purple licorice, and the residues important for cGAMP binding appear in licorice. (right) Zoomed view of the interactions with the cGAMP guanosine moiety within the binding cavity of the complexed structure. (B) Projection of the main changes of contacts in the lid region of apo STING upon G230A/R293Q double mutation (top view). Loss and gain of contacts are represented as blue and red tubes, respectively. The amino acids involved in the contacts are depicted as black beads. (C) Opening angle distributions for the (top) apo and (bottom) cGAMP-bound states of AQ-STING.

lowest value upon ligand binding. Like the A and Q variants, a drastic stiffening of the lid region is still observed in passing from the apo state to the bound state (Figures 4 and S8), correlated with changes of contacts in this region of the protein that induce a higher structuration of the β-sheet lid (Figures 6B, S5, and S6). Interestingly, the relative binding energy predicted by thermodynamic integration calculations indicates a strong perturbation leading to a lowering of the binding free energy by 9.40 ± 0.68 kcal/mol upon the AQ double mutation. Therefore, the loss of activity of AQ (or HAQ) STING might arise from both a lower affinity and lower accessibility to the binding cavity due to the stiffening of the protein structure and the more closed apo conformation.

■ CONCLUSIONS

STING is a crucial transmembrane protein that is present in the cellular ER and is involved in sensing intracellular DNA of either endogenous or exogenous origin and in triggering the immune response through proinflammatory pathways. Recently STING has also been associated with the cytokine storm that may lead to severe COVID-19 cases upon SARS-CoV-2 activation. In this contribution, by using all-atom MD simulations coupled with machine learning analysis, we have contributed to shedding light on the fundamental mechanisms of STING activation. More particularly, as the STING coding gene exhibits various polymorphisms, we have also analyzed the effects of common variants on its structural transitions and ligand binding capability with the aim to rationalize the loss of activity of some common variants. We have clearly seen that the interaction with cGAMP leads to an important remodeling of the interaction network of the protein, whose most important effect is the structuration of the disordered loops overhanging the binding pocket into a lid region assuming a β-sheet arrangement. In the WT apo form, the loops coexist in closed and open conformations, characterized by different opening angles. Obviously an open conformation is necessary to allow the entrance of cGAMP into the binding pocket and hence its recognition. Interestingly, as revealed by our PCA-based machine learning analysis, the structuration upon cGAMP binding is also accompanied by a noticeable increase in the flexibility of the linker domain involved in STING

activation via multimerization through the formation of sulfur bridges. Indeed, the cysteine residues present in the region are much more solvent-exposed as an effect of cGAMP binding, hence favoring the probability of reacting with neighboring cysteines. This long-range modulation is most probably at the base of the activation mechanism of STING, even if care should be taken to avoid overinterpretation of our results because of the use of a truncated model missing the transmembrane domain. Our results pointing to the role of the ligand-induced conformational transition are also coherent with the recent observation of Tehrani et al.[38] inferred from independent MD simulations.

Concerning the role of mutations, contrasting effects have been evidenced depending on the specific mutation. However, we may recognize a remodeling of the protein rigidity profile and internal long-range communication pathways. Indeed, changes in the flexibility of the lid region induce a perturbation of the interaction pattern within the cavity. Contrary to the A230G mutation, the R293Q mutation induces a stiffening of the lid region in both the Q and AQ models, which in turn translates into a prevalence of the closed conformation in the apo form. Of note, while the tightening of the access to the binding pocket is strongly reduced in A-STING, the simultaneous presence of the two point mutations in AQ-STING leads to an intermediate situation compared with the WT. This in turn can be related to the observed loss of efficiency of AQ-STING, which in its HAQ form is present in about 20% of the global population. Indeed, the more difficult access to the binding pocket leads to less efficient recognition of cGAMP and decreased STING activation. It is noteworthy that despite the strong remodeling of the interaction network in the lid region, the estimated binding free energy of cGAMP is only negligibly affected by the G230A mutation, while a significant increase is observed in the case of the AQ model. It is also noteworthy that ITC measurements support our results for the A variant.[31] However, the determination of experimental binding affinities for AQ and Q would be required to complement our study.

Our study allows a rationalization of the role of variants in STING contrasted phenotype and more specifically highlights the role of long-range communication and modulation of the prevalence of the open and closed conformations in cGAMP recognition and STING activation. Ergun et al.[21] compiled and critically analyzed crystal structures. They pointed out, coherently with our results, the formation of closed and more rigid arrangements. The effects of some point mutations were also taken into account, but in the majority of cases it involves the R232H allele, which despite being present in 14% of the population and responding weakly to bacterial CDNs retains a high sensitivity for cGAMP. In the future we plan to extend the study in two directions: from the one side we will focus on other variants and isoforms that are present in the general population and lead to constitutive overactivation of STING, which may be of interest in the treatment of autoimmune diseases.[25,53] On the other side, we will also increase the complexity of our model to introduce the transmembrane domain and a lipid bilayer to take into account all possible alterations of the communication network and better rationalize the enhancement of the flexibility of the linker region upon cGAMP binding. Resorting to coarse-grained approaches will also allow the explicit study of STING multimerization as well as the effect of post-translational modifications such as phosphorylation or ubiquitination, which may modulate STING activity.[54−56] A most interesting future research line would also be the study of the interaction

with viral proteases, present for instance in Zika or Dengue viruses, which reduce the host immune response by leading to the cleavage of STING.[57,58] Ultimately, the enhanced comprehension of the basic mechanisms of STING activation may lead to significant advancements in the modulation of immunotherapeutic strategies or in the development of host-targeted antiviral treatments.

■ ASSOCIATED CONTENT

Ⓢ Supporting Information

The Supporting Information is available free of charge at https://pubs.acs.org/doi/10.1021/acs.jcim.2c00315.

> Interaction network in the lid region of the WT apo STING (Figure S1); distributions of the opening angle and distance between R238 and the bottom of the cavity (Figure S2); second sphere of interaction around cGAMP (Figure S3); radial distribution of water around C148 (Figure S4); heat maps of contacts in the lid, C-terminal, and linker regions (Figures S5 and S6); binding site organization of the Q variant bound to cGAMP (Figure S7); and flexibility profiles of the variants separately (Figure S8) (PDF)

> System setup files, MD input files, analysis scripts, setup files for TI calculations, and cGAMP parameter files (ZIP)

■ AUTHOR INFORMATION

Corresponding Authors

Antonio Monari − *Université de Lorraine and CNRS, LPCT UMR 7019, F-54000 Nancy, France; Université Paris Cité and CNRS, ITODYS, F-75006 Paris, France;* ⓘ orcid.org/0000-0001-9464-1463; Email: antonio.monari@univ-lorraine.fr

Emmanuelle Bignon − *Université de Lorraine and CNRS, LPCT UMR 7019, F-54000 Nancy, France;* ⓘ orcid.org/0000-0001-9475-5049; Email: emmanuelle.bignon@univ-lorraine.fr

Authors

Jeremy Morere − *Université de Lorraine and CNRS, LPCT UMR 7019, F-54000 Nancy, France*

Cécilia Hognon − *Université de Lorraine and CNRS, LPCT UMR 7019, F-54000 Nancy, France*

Tom Miclot − *Department of Biological, Chemical and Pharmaceutical Sciences, Universita degli Studi di Palermo, 90126 Palermo, Italy; Université de Lorraine and CNRS, LPCT UMR 7019, F-54000 Nancy, France*

Tao Jiang − *Université de Lyon, ENS de Lyon, CNRS UMR 5182, Laboratoire de Chimie, F-69342 Lyon, France;* ⓘ orcid.org/0000-0002-5293-3916

Elise Dumont − *Université de Lyon, ENS de Lyon, CNRS UMR 5182, Laboratoire de Chimie, F-69342 Lyon, France; Institut Universitaire de France, F-75005 Paris, France;* ⓘ orcid.org/0000-0002-2359-111X

Giampaolo Barone − *Department of Biological, Chemical and Pharmaceutical Sciences, Universita degli Studi di Palermo, 90126 Palermo, Italy;* ⓘ orcid.org/0000-0001-8773-2359

Complete contact information is available at:
https://pubs.acs.org/10.1021/acs.jcim.2c00315

Notes

The authors declare no competing financial interest.

The supporting data described herein are available online and can also be found on our GitHub repository: https://github.com/emmanuellebignon/STINGvariants-data.

REFERENCES

(1) Ishikawa, H.; Barber, G. N. STING is an endoplasmic reticulum adaptor that facilitates innate immune signalling. *Nature* **2008**, *455*, 674−678.

(2) Sun, L.; Wu, J.; Du, F.; Chen, X.; Chen, Z. J. Cyclic GMP-AMP synthase is a cytosolic DNA sensor that activates the type I interferon pathway. *Science* **2013**, *339*, 786−791.

(3) Barber, G. N. STING: infection, inflammation and cancer. *Nat. Rev. Immunol.* **2015**, *15*, 760−770.

(4) Prantner, D.; Perkins, D. J.; Vogel, S. N. AMP-activated kinase (AMPK) promotes innate immunity and antiviral defense through modulation of stimulator of interferon genes (STING) signaling. *J. Biol. Chem.* **2017**, *292*, 292−304.

(5) Demaria, O.; De Gassart, A.; Coso, S.; Gestermann, N.; Di Domizio, J.; Flatz, L.; Gaide, O.; Michielin, O.; Hwu, P.; Petrova, T. V.; Martinon, F.; Modlin, R. L.; Speiser, D. E.; Gilliet, M. STING activation of tumor endothelial cells initiates spontaneous and therapeutic antitumor immunity. *Proc. Natl. Acad. Sci. U. S. A.* **2015**, *112*, 15408−15413.

(6) Li, A.; Yi, M.; Qin, S.; Song, Y.; Chu, Q.; Wu, K. Activating cGAS-STING pathway for the optimal effect of cancer immunotherapy. *J. Hematol. Oncol.* **2019**, *12*, 35.

(7) Motwani, M.; Pesiridis, S.; Fitzgerald, K. A. DNA sensing by the cGAS−STING pathway in health and disease. *Nat. Rev. Genet.* **2019**, *20*, 657−674.

(8) Liu, D.; Wu, H.; Wang, C.; Li, Y.; Tian, H.; Siraj, S.; Sehgal, S. A.; Wang, X.; Wang, J.; Shang, Y.; Jiang, Z.; Liu, L.; Chen, Q. STING directly activates autophagy to tune the innate immune response. *Cell Death Differ.* **2019**, *26*, 1735−1749.

(9) Vashi, N.; Bakhoum, S. F. The Evolution of STING Signaling and Its Involvement in Cancer. *Trends Biochem. Sci.* **2021**, *46*, 446−460.

(10) Mizutani, Y.; Kanbe, A.; Ito, H.; Seishima, M. Activation of STING signaling accelerates skin wound healing. *J. Dermatol. Sci.* **2020**, *97*, 21−29.

(11) Liu, Y.; Jesus, A. A.; Marrero, B.; Yang, D.; Ramsey, S. E.; Montealegre Sanchez, G. A.; Tenbrock, K.; Wittkowski, H.; Jones, O. Y.; Kuehn, H. S.; Lee, C.-C. R.; DiMattia, M. A.; Cowen, E. W.; Gonzalez, B.; Palmer, I.; DiGiovanna, J. J.; Biancotto, A.; Kim, H.; Tsai, W. L.; Trier, A. M.; Huang, Y.; Stone, D. L.; Hill, S.; Kim, H. J.; St. Hilaire, C.; Gurprasad, S.; Plass, N.; Chapelle, D.; Horkayne-Szakaly, I.; Foell, D.; Barysenka, A.; Candotti, F.; Holland, S. M.; Hughes, J. D.; Mehmet, H.; Issekutz, A. C.; Raffeld, M.; McElwee, J.; Fontana, J. R.; Minniti, C. P.; Moir, S.; Kastner, D. L.; Gadina, M.; Steven, A. C.; Wingfield, P. T.; Brooks, S. R.; Rosenzweig, S. D.; Fleisher, T. A.; Deng, Z.; Boehm, M.; Paller, A. S.; Goldbach-Mansky, R. Activated STING in a vascular and pulmonary syndrome. *N. Engl. J. Med.* **2014**, *371*, 507−518.

(12) Dobbs, N.; Burnaevskiy, N.; Chen, D.; Gonugunta, V. K.; Alto, N. M.; Yan, N. STING activation by translocation from the ER is associated with infection and autoinflammatory disease. *Cell Host Microbe* **2015**, *18*, 157−168.

(13) Berthelot, J.-M.; Lioté, F. COVID-19 as a STING disorder with delayed over-secretion of interferon-beta. *EBioMedicine* **2020**, *56*, No. 102801.

(14) Berthelot, J.-M.; Lioté, F.; Maugars, Y.; Sibilia, J. Lymphocyte changes in severe COVID-19: delayed over-activation of STING? *Front. Immunol.* **2020**, *11*, No. 607069.

(15) Neufeldt, C. J.; Cerikan, B.; Cortese, M.; Frankish, J.; Lee, J.-Y.; Plociennikowska, A.; Heigwer, F.; Prasad, V.; Joecks, S.; Burkart, S. S.; Zander, D. Y.; Subramanian, B.; Gimi, R.; Padmanabhan, S.; Iyer, R.; Gendarme, M.; El Debs, B.; Halama, N.; Merle, U.; Boutros, M.; Binder, M.; Bartenschlager, R. SARS-CoV-2 infection induces a pro-inflammatory cytokine response through cGAS-STING and NF-κB. *Commun. Biol.* **2022**, *5*, No. 45.

(16) Chin, E. N.; Yu, C.; Vartabedian, V. F.; Jia, Y.; Kumar, M.; Gamo, A. M.; Vernier, W.; Ali, S. H.; Kissai, M.; Lazar, D. C.; Nguyen, N.; Pereira, L. E.; Benish, B.; Woods, A. K.; Joseph, S. B.; Chu, A.; Johnson, K. A.; Sander, P. N.; Martinez-Pena, F.; Hampton, E. N.; Young, T. S.; Wolan, D. W.; Chatterjee, A. K.; Schultz, P. G.; Petrassi, H. M.; Teijaro, J. R.; Lairson, L. L. Antitumor activity of a systemic STING-activating non-nucleotide cGAMP mimetic. *Science* **2020**, *369*, 993−999.

(17) Humphries, F.; Shmuel-Galia, L.; Jiang, Z.; Wilson, R.; Landis, P.; Ng, S.-L.; Parsi, K.-M.; Maehr, R.; Cruz, J.; Morales, A.; Ramanjulu, J. M.; Bertin, J.; Pesiridis, G. S.; Fitzgerald, K. A. A diamidobenzimidazole STING agonist protects against SARS-CoV-2 infection. *Sci. Immunol.* **2021**, *6*, No. eabi9002.

(18) Li, S.; Luo, M.; Wang, Z.; Feng, Q.; Wilhelm, J.; Wang, X.; Li, W.; Wang, J.; Cholka, A.; Fu, Y.-x.; Sumer, B. D.; Yu, H.; Gao, J. Prolonged activation of innate immune pathways by a polyvalent STING agonist. *Nat. Biomed. Eng.* **2021**, *5*, 455−466.

(19) Pan, B.-S.; Perera, S. A.; Piesvaux, J. A.; Presland, J. P.; Schroeder, G. K.; Cumming, J. N.; Trotter, B. W.; Altman, M. D.; Buevich, A. V.; Cash, B.; Cemerski, S.; Chang, W.; Chen, Y.; Dandliker, P. J.; Feng, G.; Haidle, A.; Henderson, T.; Jewell, J.; Kariv, I.; Knemeyer, I.; Kopinja, J.; Lacey, B. M.; Laskey, J.; Lesburg, C. A.; Liang, R.; Long, B. J.; Lu, M.; Ma, Y.; Minnihan, E. C.; O'Donnell, G.; Otte, R.; Price, L.; Rakhilina, L.; Sauvagnat, B.; Sharma, S.; Tyagarajan, S.; Woo, H.; Wyss, D. F.; Xu, S.; Bennett, D. J.; Addona, G. H. An orally available non-nucleotide STING agonist with antitumor activity. *Science* **2020**, *369*, eaba6098.

(20) Shang, G.; Zhang, C.; Chen, Z. J.; Bai, X.-c.; Zhang, X. Cryo-EM structures of STING reveal its mechanism of activation by cyclic GMP−AMP. *Nature* **2019**, *567*, 389−393.

(21) Ergun, S. L.; Fernandez, D.; Weiss, T. M.; Li, L. STING polymer structure reveals mechanisms for activation, hyperactivation, and inhibition. *Cell* **2019**, *178*, 290−301.

(22) Shu, C.; Yi, G.; Watts, T.; Kao, C. C.; Li, P. Structure of STING bound to cyclic di-GMP reveals the mechanism of cyclic dinucleotide recognition by the immune system. *Nat. Struct. Mol Biol.* **2012**, *19*, 722−724.

(23) Guo, J.; Wang, J.; Fan, J.; Zhang, Y.; Dong, W.; Chen, C.-P. Distinct Dynamic and Conformational Features of Human STING in Response to 2′3′-cGAMP and c-di-GMP. *ChemBioChem* **2019**, *20*, 1838−1847.

(24) Patel, S.; Jin, L. TMEM173 variants and potential importance to human biology and disease. *Genes Immun.* **2019**, *20*, 82−89.

(25) Lin, B.; Berard, R.; Al Rasheed, A.; Aladba, B.; Kranzusch, P. J.; Henderlight, M.; Grom, A.; Kahle, D.; Torreggiani, S.; Aue, A. G.; Mitchell, J.; de Jesus, A. A.; Schulert, G. S.; Goldbach-Mansky, R. A novel STING1 variant causes a recessive form of STING-associated vasculopathy with onset in infancy (SAVI). *J. Allergy Clin. Immunol.* **2020**, *146*, 1204−1208.

(26) Lubbers, J. M.; Koopman, B.; de Klerk-Sluis, J. M.; van Rooij, N.; Plat, A.; Pijper, H.; Koopman, T.; van Hemel, B. M.; Hollema, H.; Wisman, B.; Nijman, H. W.; de Bruyn, M. Association of homozygous variants of STING1 with outcome in human cervical cancer. *Cancer Sci.* **2021**, *112*, 61−71.

(27) Ruiz-Moreno, J. S.; Hamann, L.; Shah, J. A.; Verbon, A.; Mockenhaupt, F. P.; Puzianowska-Kuznicka, M.; Naujoks, J.; Sander, L. E.; Witzenrath, M.; Cambier, J. C.; Suttorp, N.; Schumann, R. R.; Jin, L.; Hawn, T. R.; Opitz, B. The common HAQ STING variant impairs

cGAS-dependent antibacterial responses and is associated with susceptibility to Legionnaires' disease in humans. *PLoS Pathog.* **2018**, *14*, No. e1006829.

(28) Jin, L.; Xu, L.; Yang, I. V.; Davidson, E. J.; Schwartz, D. A.; Wurfel, M. M.; Cambier, J. C. Identification and characterization of a loss-of-function human MPYS variant. *Genes Immun.* **2011**, *12*, 263−269.

(29) Yi, G.; Brendel, V. P.; Shu, C.; Li, P.; Palanathan, S.; Kao, C. C. Single nucleotide polymorphisms of human STING can affect innate immune response to cyclic dinucleotides. *PLoS One* **2013**, *8*, No. e77846.

(30) Hamann, L.; Ruiz-Moreno, J. S.; Szwed, M.; Mossakowska, M.; Lundvall, L.; Schumann, R. R.; Opitz, B.; Puzianowska-Kuznicka, M. STING SNP R293Q is associated with a decreased risk of aging-related diseases. *Gerontology* **2019**, *65*, 145−154.

(31) Vavřina, Z.; Gutten, O.; Smola, M.; Zavřel, M.; Aliakbar Tehrani, Z.; Charvát, V.; Kožíšek, M.; Boura, E.; Birkuš, G.; Rulíšek, L. Protein−Ligand Interactions in the STING Binding Site Probed by Rationally Designed Single-Point Mutations: Experiment and Theory. *Biochemistry* **2021**, *60*, 607−620.

(32) Smola, M.; Gutten, O.; Dejmek, M.; Kožíšek, M.; Evangelidis, T.; Tehrani, Z. A.; Novotná, B.; Nencka, R.; Birkuš, G.; Rulíšek, L.; Boura, E. Ligand Strain and Its Conformational Complexity Is a Major Factor in the Binding of Cyclic Dinucleotides to STING Protein. *Angew. Chem.* **2021**, *133*, 10260−10266.

(33) Shih, A. Y.; Damm-Ganamet, K. L.; Mirzadegan, T. Dynamic structural differences between human and mouse STING lead to differing sensitivity to DMXAA. *Biophys. J.* **2018**, *114*, 32−39.

(34) Che, X.; Du, X.-X.; Cai, X.; Zhang, J.; Xie, W. J.; Long, Z.; Ye, Z.-Y.; Zhang, H.; Yang, L.; Su, X.-D.; Gao, Y. Q. Single mutations reshape the structural correlation network of the DMXAA−human STING complex. *J. Phys. Chem. B* **2017**, *121*, 2073−2082.

(35) Gao, P.; Zillinger, T.; Wang, W.; Ascano, M.; Dai, P.; Hartmann, G.; Tuschl, T.; Deng, L.; Barchet, W.; Patel, D. J. Binding-pocket and lid-region substitutions render human STING sensitive to the species-specific drug DMXAA. *Cell Rep.* **2014**, *8*, 1668−1676.

(36) Che, X.; Zhang, J.; Quan, H.; Yang, L.; Gao, Y. Q. CDNs−STING Interaction Mechanism Investigations and Instructions on Design of CDN-Derivatives. *J. Phys. Chem. B* **2018**, *122*, 1862−1868.

(37) Zhong, S.; Li, W.; Bai, Y.; Wu, B.; Wang, X.; Jiang, S.; Zhao, Y.; Ren, J.; Li, H.; Jin, R. Computational study on new natural compound agonists of stimulator of interferon genes (STING). *PLoS One* **2019**, *14*, No. e0216678.

(38) Tehrani, Z. A.; Rulíšek, L.; Černý, J. Molecular dynamics simulations provide structural insight into binding of cyclic dinucleotides to human STING protein. *J. Biomol. Struct. Dyn.* **2021**, DOI: 10.1080/07391102.2021.1942213. PMID: 34187319

(39) Waterhouse, A.; Bertoni, M.; Bienert, S.; Studer, G.; Tauriello, G.; Gumienny, R.; Heer, F. T.; de Beer, T. A. P.; Rempfer, C.; Bordoli, L.; Lepore, R.; Schwede, T. SWISS-MODEL: homology modelling of protein structures and complexes. *Nucleic Acids Res.* **2018**, *46*, W296−W303.

(40) Zhang, X.; Shi, H.; Wu, J.; Zhang, X.; Sun, L.; Chen, C.; Chen, Z. J. Cyclic GMP-AMP Containing Mixed Phosphodiester Linkages Is An Endogenous High-Affinity Ligand for STING. *Mol. Cell* **2013**, *51*, 226−235.

(41) Case, D. A.; Ben-Shalom, I. Y.; Brozell, S. R.; Cerutti, D. S.; Cheatham, T. E., III; Cruzeiro, V. W. D.; Darden, T. A.; Duke, R. E.; Ghoreishi, D.; Gilson, M. K.; Gohlke, H.; Goetz, A. W.; Greene, D.; Harris, R.; Homeyer, N.; Huang, Y.; Izadi, S.; Liu, J.; Luchko, T.; Luo, R.; Mermelstein, D. J.; Merz, K. M.; Miao, Y.; Monard, G.; Nguyen, C.; Nguyen, H.; Omelyan, I.; Onufriev, A.; Pan, F. J.; Qi, R.; Roe, D. R.; Roitberg, A.; Sagui, C.; Schott-Verdugo, S.; Shen, J.; Simmerling, C. L.; Smith, J.; Salomon-Ferrer, R.; Swails, J.; Walker, R. C.; Wang, J.; Wei, H.; Wolf, R. M.; Wu, X.; Xiao, L; York, D. M.; Kollman, P. A. *AMBER 2018*; University of California: San Francisco, 2018.

(42) Bayly, C. I.; Cieplak, P.; Cornell, W.; Kollman, P. A. A well-behaved electrostatic potential based method using charge restraints for deriving atomic charges: the RESP model. *J. Phys. Chem.* **1993**, *97*, 10269−10280.

(43) Wang, J.; Wolf, R. M.; Caldwell, J. W.; Kollman, P. A.; Case, D. A. Development and testing of a general amber force field. *J. Comput. Chem.* **2004**, *25*, 1157−1174.

(44) Maier, J. A.; Martinez, C.; Kasavajhala, K.; Wickstrom, L.; Hauser, K. E.; Simmerling, C. ff14SB: improving the accuracy of protein side chain and backbone parameters from ff99SB. *J. Chem. Theory Comput.* **2015**, *11*, 3696−3713.

(45) Phillips, J. C.; Hardy, D. J.; Maia, J. D. C.; Stone, J. E.; Ribeiro, J. V.; Bernardi, R. C.; Buch, R.; Fiorin, G.; Hénin, J.; Jiang, W.; McGreevy, R.; Melo, M. C. R.; Radak, B. K.; Skeel, R. D.; Singharoy, A.; Wang, Y.; Roux, B.; Aksimentiev, A.; Luthey-Schulten, Z.; Kalé, L. V.; Schulten, K.; Chipot, C.; Tajkhorshid, E. Scalable molecular dynamics on CPU and GPU architectures with NAMD. *J. Chem. Phys.* **2020**, *153*, 044130.

(46) Essmann, U.; Perera, L.; Berkowitz, M. L.; Darden, T.; Lee, H.; Pedersen, L. G. A smooth particle mesh Ewald method. *J. Chem. Phys.* **1995**, *103*, 8577−8593.

(47) Wickham, H. *ggplot2: Elegant Graphics for Data Analysis*; Springer: New York, 2009.

(48) Humphrey, W.; Dalke, A.; Schulten, K. VMD: visual molecular dynamics. *J. Mol. Graphics* **1996**, *14*, 33−38.

(49) Fleetwood, O.; Kasimova, M. A.; Westerlund, A. M.; Delemotte, L. Molecular Insights from Conformational Ensembles via Machine Learning. *Biophys. J.* **2020**, *118*, 765−780.

(50) Bignon, E.; Claerbout, V. E.; Jiang, T.; Morell, C.; Gillet, N.; Dumont, E. Nucleosomal embedding reshapes the dynamics of abasic sites. *Sci. Rep.* **2020**, *10*, No. 17314.

(51) Bignon, E.; Gillet, N.; Jiang, T.; Morell, C.; Dumont, E. A Dynamic View of the Interaction of Histone Tails with Clustered Abasic Sites in a Nucleosome Core Particle. *J. Phys. Chem. Lett.* **2021**, *12*, 6014−6019.

(52) Bignon, E.; Gillet, N.; Chan, C.-H.; Jiang, T.; Monari, A.; Dumont, E. Recognition of a tandem lesion by DNA bacterial formamidopyrimidine glycosylases explored combining molecular dynamics and machine learning. *Comput. Struct. Biotechnol. J.* **2021**, *19*, 2861−2869.

(53) Wang, P.-H.; Fung, S.-Y.; Gao, W.-W.; Deng, J.-J.; Cheng, Y.; Chaudhary, V.; Yuen, K.-S.; Ho, T.-H.; Chan, C.-P.; Zhang, Y.; Kok, K.-H.; Yang, W.; Chan, C.-P.; Jin, D.-Y. A novel transcript isoform of STING that sequesters cGAMP and dominantly inhibits innate nucleic acid sensing. *Nucleic Acids Res.* **2018**, *46*, 4054−4071.

(54) Zhang, J.; Hu, M.-M.; Wang, Y.-Y.; Shu, H.-B. TRIM32 protein modulates type I interferon induction and cellular antiviral response by targeting MITA/STING protein for K63-linked ubiquitination. *J. Biol. Chem.* **2012**, *287*, 28646−28655.

(55) Konno, H.; Konno, K.; Barber, G. N. Cyclic dinucleotides trigger ULK1 (ATG1) phosphorylation of STING to prevent sustained innate immune signaling. *Cell* **2013**, *155*, 688−698.

(56) Hansen, A. L.; Mukai, K.; Schopfer, F. J.; Taguchi, T.; Holm, C. K. STING palmitoylation as a therapeutic target. *Cell. Mol. Immunol.* **2019**, *16*, 236−241.

(57) Ding, Q.; Gaska, J. M.; Douam, F.; Wei, L.; Kim, D.; Balev, M.; Heller, B.; Ploss, A. Species-specific disruption of STING-dependent antiviral cellular defenses by the Zika virus NS2B3 protease. *Proc. Natl. Acad. Sci. U. S. A.* **2018**, *115*, E6310−E6318.

(58) Su, C.-I.; Kao, Y.-T.; Chang, C.-C.; Chang, Y.; Ho, T.-S.; Sun, H. S.; Lin, Y.-L.; Lai, M. M.; Liu, Y.-H.; Yu, C.-Y. DNA-induced 2′3′-cGAMP enhances haplotype-specific human STING cleavage by dengue protease. *Proc. Natl. Acad. Sci. U. S. A.* **2020**, *117*, 15947−15954.